INDIVIDUAL NODULE TRACKING IN MICRO-CT IMAGES OF A MOUSE MODEL OF LUNG CANCER

Rina D. Rudyanto, Ainhoa Agirre, Carlos Ortiz-de-Solorzano, Arrate Munoz-Barrutia

Center for Applied Medical Research, University of Navarra, Pamplona, Spain

ABSTRACT

We present an automatic method to track individual nodule progression in a lung cancer mouse model. Fourteen A/J mice received an intraperitoneal injection of urethane. Respiratory-gated micro-CT images of the lungs were taken 8, 22, and 37 weeks after injection, at which 195, 585 and 636 nodules were manually detected. The three images from every animal were registered and their nodules matched with average accuracy of 97.2%. All nodules detected at week 8 were then tracked until week 37, and volumetrically segmented to characterize the growth rate and doubling rate. Our framework is able to segment 92.9% of all nodules, ranging from the earliest stage (0.2mm) to advanced stage where nodule segmentation becomes challenging due to complex anatomy and nodule overlap. In conclusion, we showed the utility of the proposed framework to facilitate further research in pre-clinical lung cancer model.

Index Terms— micro-CT, animal model, lung cancer, longitudinal studies, nodule segmentation

1. INTRODUCTION

Lung cancer is the leading cause of cancer-related deaths worldwide [1]; therefore, early detection and accurate differential diagnosis of suspicious lung lesions is critical to reduce mortality. Computed tomography (CT) has been demonstrated a useful tool for non-invasive detection of lung cancer in clinical settings. In preclinical studies, imaging using micro-CT offers the ability to perform longitudinal studies of disease models. Being non-invasive, this novel approach gives the ability to gain insight into disease progression, to monitor therapeutic effects and to optimize the experimental period while minimizing the number of animals necessary. However, there are also disadvantages in that some radiation is delivered in each scan and the image quality is strongly compromised by motion-related artifacts. To increase image quality, we have combined respiratory gating with animal intubation and artificial ventilation, to provide high-resolution micro-CT imaging of an almost motion-free lung during controlled breath-holds. Using this protocol we have been able to quantitatively characterize several models of lung disease longitudinally [2].

There are several models of lung cancer, which can be used to study the biology of the disease and the effect of novel therapeutic drugs. In one such model, lung lesions are induced by intraperitoneal injection of urethane in male A/J mice. Nodule progression in this model has been assessed longitudinally [3,4]. Growth of individual nodules have been tracked manually using interactive commercial software for both lung registration and nodule segmentation. Furthermore, nodule growth has only been studied up to a limited extent in models provoked by low urethane dosage [4] or studied over short-term period [3].

In this paper, we present a fully automatic, open-source single-pipeline framework that integrates all the steps needed for the longitudinal characterization of individual nodules starting from nodule detection. The algorithm volumetrically segments the nodules starting from interactively planted seeds, and tracks their evolution in time after proper registration of the lungs. The outcome is a detailed characterization of individual nodule's growth and doubling rate. We believe that the relevance of the urethane-induced model in pre-clinical studies justifies the development of this tool to arrive at an accurate and reproducible quantitative picture of the evolution of the disease.

The manuscript is organized as follows: In Section 2, we describe the animal imaging protocol and the algorithm developed to characterize the nodules. In Section 3, we present the results of an experiment on growth rate of lung nodules. In Section 4, we discuss the challenges and future extensions.

2. MATERIAL AND METHODS

2.1. Animal preparation and image acquisition

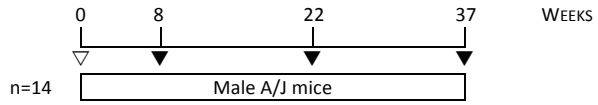


Fig. 1: Experiment Design. ▽Urethane injection ▼micro-CT scan

The experimental protocol is shown in Fig. 1. Fourteen male A/J mice received a single intraperitoneal injection of urethane (100mg/100g). Then 8, 22, and 37 weeks after urethane administration, all mice underwent respiratory-gated micro-CT scans. To this end, each mouse was anaesthetized, endotracheally intubated, connected to a

Flexivent rodent ventilator (Scireq, Montreal, Canada) and kept breathing isoflurane at 2% concentration until complete relaxation state, after which isoflurane concentration was reduced to 0.5% and maintained at that level during the rest of the experiment. Then the animals were scanned with a Micro-CAT II (Siemens Pre-Clinical Solutions, Knoxville, Tennessee) XRay microCT, with a source voltage of 80 kVp and a current of 500 μA. Seven hundred projections were acquired during 650 ms iso-pressure peak inspiration breath holds, with an exposure time of 450 ms per projection. The average scan time was 32 minutes, and the dosage as computed by the Dose Calculator software (Siemens Pre-Clinical Solutions, Knoxville, Tennessee) was 71.6 cGy per scan. All images were calibrated to Hounsfield Units (HU) using a water phantom. After the last time point, the animals were sacrificed, and their lungs were collected for histology.

2.2. Image Analysis

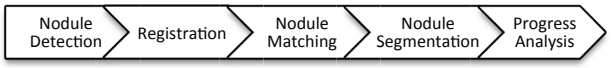


Fig. 2: Overview of the steps of nodule growth analysis

The main steps required to characterize nodule progression are summarized in Fig. 2.

Nodule Detection: All micro-CT images were analyzed by a radiologist, who used ImageJ plug-in PointPicker [5] to detect all nodules.

Registration: The lungs segmented in three images of each animal were registered pairwise (week 8 & 22, week 22 & 37) using elastix [6]. Lung segmentation was performed using the method described by Hu *et al.* [7], followed by a morphological closing operation destined to include nodules attached to pleural areas. An affine transformation was then applied, followed by an elastic B-spline transformation using an isotropic grid spacing of 8.0 pixels. In both registration steps, mutual information was maximized using a multiscale stochastic gradient descent optimizer with three resolution levels. The registration was evaluated using the Similarity Index (overlap between two images) and validated by calculating the mean Euclidean distance between the locations of anatomical landmarks (carina, left lung apex, right lung apex) manually marked using PointPicker.

Nodule Matching: Each nodule position marked by the radiologist was then transformed according with the output of the registration step and matched to the closest nodule in the next time point. The possibility of two nodules matched to the same nodule in the next image is permitted as the growing tumors might overlap, forming clusters.

Nodule Segmentation: Each nodule was automatically segmented in 3D using seeded region growing from the location previously identified by the radiologist, within a predefined volume of interest (VOI).

Segmentation can be achieved using simple thresholding for *well-circumscribed*, isolated nodules. Nodules growing next to the chest wall (*juxtapleural*) or vasculature (*juxtavascular*), are more challenging and require an additional processing described in Fig. 3 adapted from [8,9] to separate the actual nodule region from its surrounding anatomical structures. The sequence of operations we chose to segment all the nodules is as follows: (1) a VOI is calculated with the seed at the center, (2) binary segmentation with the initial threshold is performed, (3) the intersection of the binary segmentation with the convex hull of its complement is calculated, (4) then eroded and dilated, (5) and finally a 2-D binary connected thresholding starting from the seed is applied. A pilot experiment was used to define the optimal segmentation parameters. The initial threshold is -300HU (mean of 50 HU and -750HU, which is typical of nodule and parenchyma, respectively). The mean value between the initial threshold and the pixel value at the seed is used when the latter is lower than the initial threshold. The small cubic VOI is of size 30, 55, 60 pixels for weeks 8, 22 and 37, respectively.

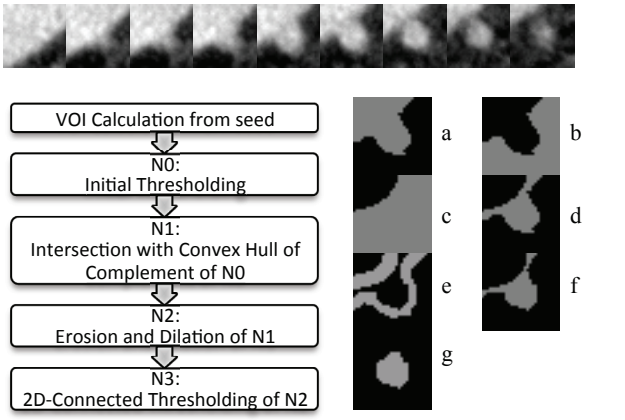


Fig. 3: (top) Image of nodule attached to the heart, from top slice to bottom; (bottom left) Sequential steps in nodule segmentation to separate nodule region from chest wall or cardiovascular areas; (bottom right) Output from each step shown for slice containing seed: (a) N0: initial thresholding; (b) complement of (a); (c) convex hull of (b); (d) N1: intersection of (a) and (c); (e) N2: erosion & dilation of boundary of (d); (f) subtracting (e) with (a); (g) N3: final result after morphological closing and 2D-connected thresholding of (f).

Using a fixed large VOI size for nodules in week 37 generally results in inclusion of more than one seed in a single VOI. When this happens, an adaptive VOI is recalculated before the segmentation was performed: a slice-by-slice 2D binary thresholding [9] from the seed was used to determine the area of the foreground region. Starting from the slice that contains the seed, the extent of the VOI in the axial direction is found when there are at least two sides not in contact with the foreground area. Along the superior-inferior axis, a decrease of more than 10% in the foreground area marks the end of VOI in the case of well-circumscribed nodules and an increase of more than 5% marks the end of VOI in the case of juxtapleural nodules.

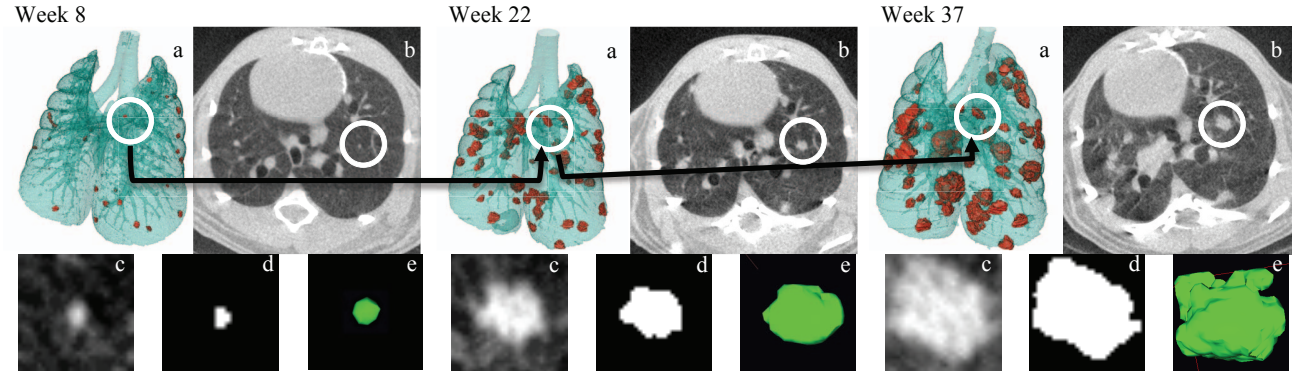


Fig. 1. For week 8, 22 and 37: (a) 3-D Reconstruction of lung and nodules (example nodule at different time points indicated with white circle); (b) CT scan slice including the nodule chosen as example; (c) Nodule Volume of Interest; (d) Binary segmented nodule; (e) Nodule 3-D reconstruction.

The automatic segmentation method was evaluated against the manual segmentation performed by two-observers using the Amira software (Visage Imaging, Fürth, Germany). The evaluation was done using two animals at all three time points. The segmented tumor overlap and total tumor volume were used as metrics.

Progress Analysis: All nodules identified at week 8 were then tracked. Nodule progression analysis was done comparing volumes, growth rate and doubling rate.

3. RESULTS

Fig. 1 shows a 3-D reconstruction of the whole lung and cancerous nodules as well as an example of a nodule tracked in time.

Nodule Detection: The number of nodules detected is shown in Table 1. In all but four animals, the number of nodules increased between week 22 and 37.

Week	Tumors detected (in 14 animals)	
	Total Tumors	No. of tumors/mouse (mean±stdev)
8	195	13.93±6.23
22	585	41.86±10.90
37	636	45.43±8.38

Table 1. Incidence and multiplicity of nodules detected.

Registration: The evaluation of the registration showed average Similarity Index value of 0.93 between the images at week 8 and 22, and 0.92 between week 22 and 37. The Mean Euclidean distance between anatomical landmarks and their respective transformed points is given in Table 2.

Time Points	Average Mean Distance (pixels)		
	Carina	$Apex_{Right}$	$Apex_{Left}$
Week 8 to 22	17.16±8.35	10.84±6.63	12.06±7.90
Week 22 to 37	20.34±10.10	16.55±8.07	18.98±8.73

Table 2. Registration error given by average mean distance.

Nodule Matching: The accuracy of nodule matching was manually corroborated: 97.4% accurate matching is obtained between week 8 and 22, and 96.9% between week 22 and 37. One nodule was not manually detected and six nodule mismatches occurred. The result after matching is shown in Fig. 2.

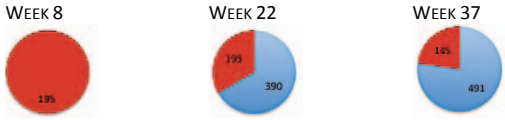


Fig. 2. Clusters after matching: 195 nodules at week 8, matched to 195 nodules at week 22, which then matched to 145 clusters at week 37.

Nodule Segmentation: The number of nodules successfully segmented is shown in Table 3.

Week	Tumors detected (in 14 animals)	
	Total Tumors detected	No. of tumors segmented
8	195	188 (96.4%)
22	585	548 (93.6%)
37	636	580 (84.5%)
Total	1316	1416 (92.9%)

Table 3. Number of tumors successfully segmented.

The average Similarity Index between the automatic segmentation method and the manual segmentation done by two independent observers was 0.88. The average Similarity Index between manual observers was 0.69. The differences in total segmented tumor volume are shown in Table 4.

		Total Tumor Volume (μL)		
	Week	Observer #1	Observer #2	Automatic
Animal 1	8	2.14	1.69	1.43
	22	11.05	12.18	8.77
	37	26.01	31.47	28.76
Animal 2	8	0.95	1.55	0.88
	22	18.90	20.41	17.19
	37	103.31	65.67	68.15

Table 4. Average difference of total tumor volume between automatic method and manual observers performed on two animals.

Progress Analysis: The total tumor growth rate and doubling rate were calculated for the two different periods, as shown in Table 5.

Period	Growth Rate (mean±std, µL/week)	Doubling Rate (mean±std, in weeks)
Week 8 to 22	0.02±0.006	5.71±1.57
Week 22 to 37	0.07±0.03	7.88±2.16

Table 5. Tumor growth and doubling rate of the tumors detected at all three time points (n=195).

Analyzing nodules individually enables characterization of different growth rates, suggesting the presence of distinct populations – slow growing and fast growing nodules. An example of clusters growing at different rates in one animal, is shown in Fig. 3.

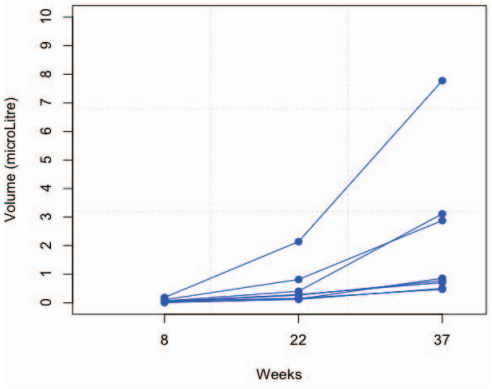


Fig. 3. Volume of nodule clusters in one animal across three time points.

4. DISCUSSION

We have presented an automated framework for tracking the growth of individual lung nodules in a mouse model of lung cancer induced by urethane. Combining image registration and image segmentation, we are able to study nodule growth, starting as early as 8 weeks –the smallest nodule measuring 0.2 mm in diameter– until an advanced stage at 37 weeks.

Registration is somewhat less accurate than expected in human cases. At advanced stages, breathing became laborious. Consequently, given the large duration of the scan, breath hold intubation technique does not completely eliminate motion artifacts, resulting in poorer image quality.

Nodule segmentation in small animal imaging is challenging when the nodules are attached to the pleura or vascular structures, and especially so at advanced stages, when multiple nodules collapse into complex tumor clusters. The complexity of this task is not immediately apparent when dealing with human cases, which tend to have smaller number of isolated nodules. In this paper we have presented a robust segmentation that successfully deals with the particularities.

The task of manually detecting, segmenting and tracking nodules is too labor intensive to be practical in a real experimental setting. Consequentially, we plan to incorporate automatic detection of the nodules to our framework.

Studying growth without tracking individual nodules may miss valuable information such as the relationship between nodule progression and regional anatomies, and the progression with respect to nodule onset. Supported with a proper histological characterization of tumors, our approach of individual nodule tracking, could be used to discover image biomarkers (e.g. growth rates, doubling rates, average HU, spiked edges/clear margins) that describe different phenotypes of tumors. Future medical utility includes animal study of the effectiveness of novel anti-tumoral therapies targeted at specific cancer phenotype.

5. REFERENCES

[1] RS Herbst, JV Heymach, and SM Lippman, "Lung cancer," *N Engl J Med*, vol. 359, no. 13, pp. 1367-1380, 2008.

[2] X Artaechevarria et al., "Evaluation of micro-CT for emphysema assessment in mice: comparison with non-radiological techniques," *Eur Radiol*, vol. 21, no. 5, pp. 954-962, 2011.

[3] E Namati et al., "Longitudinal assessment of lung cancer progression in the mouse using in vivo micro-CT imaging," *Med Phys*, vol. 37, pp. 4793-4805, 2010.

[4] Y Hori et al., "Periodic analysis of urethane-induced pulmonary tumors in living A/J mice by respiration-gated X-ray microcomputed tomography," *Cancer Science*, vol. 99, no. 9, pp. 1774-1777, 2008.

[5] P Thevenaz. PointPicker. [Online]. http://bit.ly/tjWKLS

[6] S. Klein, M Staring, K Murphy, M Viergever, and J. Pluim, "elastix: a toolbox for intensity-based medical image registration," *IEEE Trans Med Imaging*, vol. 29, no. 1, pp. 196-205, 2010.

[7] S Hu, E. Hoffman, and J. Reinhardt, "Automatic lung segmentation for accurate quantitation of volumetric X-ray CT images," *IEEE Trans Med Imaging*, vol. 20, no. 6, pp. 490-498, 2001.

[8] JM Kuhnigk et al., "Morphological segmentation and partial volume analysis for volumetry of solid pulmonary lesions in thoracic CT scans," *IEEE Trans Med Imaging*, vol. 25, no. 4, pp. 417-434, 2006.

[9] J Dehmeshki, H Amin, M Valdivieso, and X. Ye, "Segmentation of pulmonary nodules in thoracic CT scans: a region growing approach.," *IEEE Trans Med Imaging*, vol. 27, no. 4, pp. 467-480, 2008.

6. ACKNOWLEDGEMENT

This work has partially been supported by the UTE Project CIMA and the Spanish Science and Innovation Ministry (MICINN) under grants PSS-010000-2008-2 and DPI2009-14115-C03-03. A. Muñoz-Barrutia and C. Ortiz-de-Solórzano hold a Ramón y Cajal fellowship of the MICINN.